

Signatures of Majorana Fermions in Hybrid Superconductor-Semiconductor Nanowire Devices

V. Mourik,^{1*} K. Zuo,^{1*} S. M. Frolov,¹ S. R. Plissard,² E. P. A. M. Bakkers,^{1,2} L. P. Kouwenhoven^{1†}

¹Kavli Institute of Nanoscience, Delft University of Technology, 2600 GA Delft, Netherlands.

²Department of Applied Physics, Eindhoven University of Technology, 5600 MB Eindhoven, Netherlands.

*These authors contributed equally to this work.

†To whom correspondence should be addressed. E-mail: l.p.kouwenhoven@tudelft.nl

Majorana fermions are particles identical to their own antiparticles. They have been theoretically predicted to exist in topological superconductors. We report electrical measurements on InSb nanowires contacted with one normal (Au) and one superconducting electrode (NbTiN). Gate voltages vary electron density and define a tunnel barrier between normal and superconducting contacts. In the presence of magnetic fields of order 100 mT we observe bound, mid-gap states at zero bias voltage. These bound states remain fixed to zero bias even when magnetic fields and gate voltages are changed over considerable ranges. Our observations support the hypothesis of Majorana fermions in nanowires coupled to superconductors.

All elementary particles have an antiparticle of opposite charge (for example, an electron and a positron); the meeting of a particle with its antiparticle results in the annihilation of both. A special class of particles, called Majorana fermions, are predicted to exist that are identical to their own antiparticle (1). They may appear naturally as elementary particles, or emerge as charge-neutral and zero-energy quasi-particles in a superconductor (2, 3). Particularly interesting for the realization of qubits in quantum computing are pairs of localized Majoranas separated from each other by a superconducting region in a topological phase (4–11).

Based on earlier semiconductor-based proposals, (6) and later (7), Lutchyn *et al.* (8) and Oreg *et al.* (9) have outlined the necessary ingredients for engineering a nanowire device that should accommodate pairs of Majoranas. The starting point is a one-dimensional nanowire made of semiconducting material with strong spin-orbit interaction (Fig. 1A). In the presence of a magnetic field, B , along the axis of the nanowire (i.e., a Zeeman field), a gap is opened at the crossing between the two spin-orbit bands. If the Fermi energy, μ , is inside this gap, the degeneracy is two-fold whereas outside the gap it is four-fold. The next ingredient is to connect the semiconducting nanowire to an ordinary s -wave superconductor (Fig. 1A). The proximity of the superconductor induces pairing in the nanowire between electron states of opposite momentum and opposite spins and induces a gap, Δ . Combining this two-fold degeneracy with an induced gap creates a topological superconductor (4–11). The condition for a topological phase is $E_Z > (\Delta^2 + \mu^2)^{1/2}$, with the Zeeman energy, $E_Z = g\mu_B B/2$ (g is the Landé g -factor; μ_B the Bohr magneton). Near the ends of the wire, the electron density is reduced to zero and subsequently μ will drop below the subband energies such that μ^2 becomes large. At the points in space where $E_Z = (\Delta^2 + \mu^2)^{1/2}$ Majoranas arise as zero-energy (i.e., mid-gap) bound states—one at each end of the wire (4, 8–11).

Despite their zero charge and energy, Majoranas can be detected in electrical measurements. Tunneling spectroscopy from a normal conductor into the end of the wire should reveal a state at zero energy (12–14).

enter the topological phase for $B \sim 0.15$ T where E_Z starts to exceed Δ . The energy gap of the topological superconductor is estimated to be a few Kelvin (17), if we assume a ballistic nanowire. The topological gap is significantly reduced in a disordered wire (18, 19). We have measured mean free paths of ~ 300 nm in our wires (15), implying a quasi-ballistic regime in micrometer long wires. With these numbers we expect Majorana zero-energy states to become observable below one Kelvin and around 0.15 T.

A typical sample is shown in Fig. 1B. We first fabricate a pattern of narrow (50 nm) and wider (300 nm) gates on a silicon substrate (20). The gates are covered by a thin Si_3N_4 dielectric before we randomly deposit a low density of InSb nanowires. Next, we electrically contact those nanowires that have landed properly relative to the gates. The lower contact in Fig. 1B fully covers the bottom part of the nanowire. We have designed the upper contact to only cover half of the top part of the nanowire, avoiding complete screening of the underlying gates. This allows us to change the Fermi energy in the section of the nanowire (NW) with induced superconductivity. We have used either a normal (N) or superconducting (S) material for the lower and upper contacts, resulting in three sample variations: N-NW-S, N-NW-N and S-NW-S. Here we discuss our main results on the N-NW-S devices whereas the other two types, serving as control devices, are described in (20).

To perform spectroscopy on the induced superconductor we create a tunnel barrier in the nanowire by applying a negative voltage to a narrow gate (dark green gate in Fig. 1, B and C). A bias voltage applied externally between the N and S contacts drops almost completely across the tunnel barrier. In this setup the differential conductance dI/dV at voltage V is proportional to the density of states at energy $E = eV$, relative to the zero-energy, dashed line in Fig. 1C. Figure 1D shows an example taken at $B = 0$. The two peaks at ± 250 μeV correspond to the peaks in the quasi-particle density of states of the induced superconductor, providing a value for the induced gap, $\Delta \approx 250$ μeV . We generally find a finite dI/dV in between these gap edges. We observe pairs of resonances with energies symmetric around zero bias superimposed on non-resonant currents

Here we report the observation of such zero-energy peaks and show that they rigidly stick to zero-energy while changing B and gate voltages over large ranges. Furthermore, we show that this zero-bias peak is absent if we take out any of the necessary ingredients of the Majorana proposals, i.e., the rigid zero bias peak disappears for zero magnetic field, for a magnetic field parallel to the spin-orbit field, or when we take out the superconductivity.

We use InSb nanowires (15), which are known to have strong spin-orbit interaction and a large g -factor (16). From our earlier quantum dot experiments we extract a spin-orbit length $l_{\text{so}} \approx 200$ nm corresponding to a Rashba parameter $\alpha \approx 0.2$ eV $\cdot\text{\AA}$ (17). This translates to a spin-orbit energy scale $\alpha^2 m^*/(2\hbar^2) \approx 50$ μeV ($m^* = 0.015m_e$ is the effective electron mass in InSb, m_e is the bare electron mass). Importantly, the g -factor in bulk InSb is very large, $g \approx 50$, yielding $E_Z/B \approx 1.5$ meV/T. As shown below, we find an induced superconducting gap $\Delta \approx 250$ μeV . For $\mu = 0$ we thus expect to

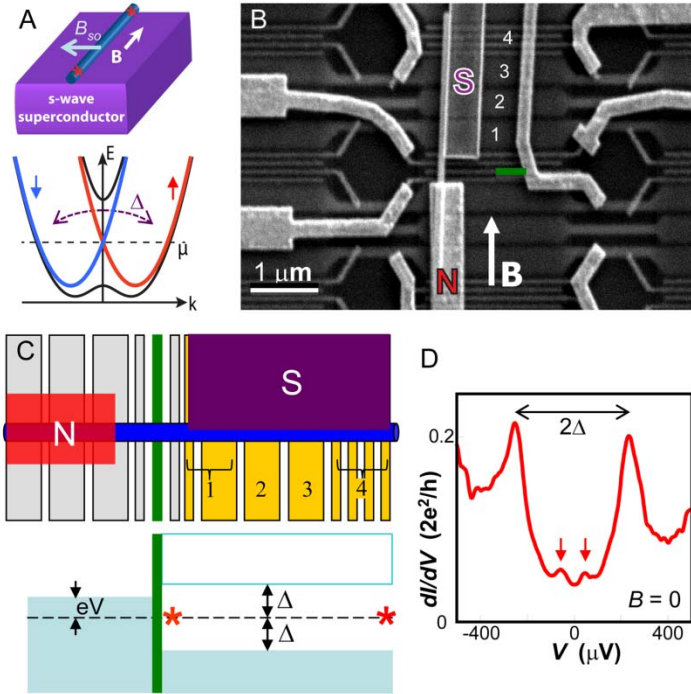


Fig. 1. (A) Outline of theoretical proposals. (Top) Conceptual device layout with a semiconducting nanowire in proximity to an s-wave superconductor. An external B -field is aligned parallel to the wire. The Rashba spin-orbit interaction is indicated as an effective magnetic field, B_{so} , pointing perpendicular to the nanowire. The red stars indicate the expected locations of a Majorana pair. (Bottom) Energy, E , versus momentum, k , for a 1D wire with Rashba spin-orbit interaction, which shifts the spin-down band (blue) to the left and spin-up band (red) to the right. Blue and red parabolas are for $B = 0$. Black curves are for $B \neq 0$, illustrating the formation of a gap near $k = 0$ of size $g\mu_B B$. (μ is the Fermi energy with $\mu = 0$ defined at crossing of parabolas at $k = 0$). The superconductor induces pairing between states of opposite momentum and opposite spin creating a gap of size Δ . (B) Implemented version of theoretical proposals. Scanning electron microscope image of the device with normal (N) and superconducting (S) contacts. The S-contact only covers the right part of the nanowire. The underlying gates, numbered 1 to 4, are covered with a dielectric. [Note that gate 1 connects two gates and gate 4 connects four narrow gates; see (C).] (C) (Top) Schematic of our device. (Down) illustration of energy states. Green indicates the tunnel barrier separating the normal part of the nanowire on the left from the wire section with induced superconducting gap, Δ . [In (B) the barrier gate is also marked green.] An external voltage, V , applied between N and S drops across the tunnel barrier. Red stars again indicate the idealized locations of the Majorana pair. Only the left Majorana is probed in this experiment. (D) Example of differential conductance, dI/dV , versus V at $B = 0$ and 65 mK, serving as a spectroscopic measurement on the density of states in the nanowire region below the superconductor. Data from device 1. The two large peaks, separated by 2Δ , correspond to the quasi-particle singularities above the induced gap. Two smaller subgap peaks, indicated by arrows, likely correspond to Andreev bound states located symmetrically around zero energy. Measurements are performed in dilution refrigerators using standard low-frequency lock-in technique (frequency 77 Hz, excitation 3 μ V) in the four-terminal (devices 1 and 3) or two-terminal (device 2) current-voltage geometry.

throughout the gap region. Symmetric resonances likely originate from Andreev bound states (21, 22), whereas non-resonant current indicates that the proximity gap has not fully developed (23).

Figure 2 summarizes our main result. Figure 2A shows a set of dI/dV versus V traces taken at increasing B -fields in 10 mT steps from zero (lowest trace) to 490 mT (top trace), offset for clarity. We again observe the gap edges at $\pm 250 \mu\text{eV}$. When we apply a B -field between ~ 100 and ~ 400 mT along the nanowire axis we observe a peak at $V = 0$. The peak has an amplitude up to $\sim 0.05 \cdot 2e^2/h$ and is clearly discernible from the background conductance. Above ~ 400 mT we observe a pair of peaks. The color panel in Fig. 2B provides an overview of states and gaps in the plane of energy and B -field from -0.5 to 1 T. The observed symmetry around $B = 0$ is typical for all our data sets, demonstrating reproducibility and the absence of hysteresis. We indicate the gap edges with horizontal dashed lines (highlighted only for $B < 0$). A pair of resonances crosses zero energy at ~ 0.65 T with a slope of order E_z (highlighted by dotted lines). We have followed these resonances up to high bias voltages in (20) and identified them as Andreev states bound within the gap of the bulk, NbTiN superconducting electrodes (~ 2 meV). By contrast, the zero-bias peak sticks to zero energy over a range of $\Delta B \sim 300$ mT centered around ~ 250 mT. Again at ~ 400 mT we observe two peaks located at symmetric, finite biases.

In order to identify the origin of these zero-bias peaks (ZBP) we need to consider various options, including the Kondo effect, Andreev bound states, weak antilocalization and reflectionless tunneling, versus a conjecture of Majorana bound states. ZBPs due to the Kondo effect (24) or Andreev states bound to s-wave superconductors (25) can occur at finite B . However, when changing B these peaks then split and move to finite energy. A Kondo resonance moves with twice E_z (24), which is easy to dismiss as the origin for our zero-bias peak because of the large g -factor in InSb. (Note that even a Kondo effect from an impurity with $g = 2$ would be discernible.) Reflectionless tunneling is an enhancement of Andreev reflection by time-reversed paths in a diffusive normal region (26). As in the case of weak antilocalization, the resulting ZBP is maximal at $B = 0$ and disappears when B is increased, see also (20). We thus conclude that the above options for a ZBP do not provide natural explanations for our observations. We are not aware of any mechanism that

could explain our observations, besides the conjecture of a Majorana.

To further investigate the zero-biasness of our peak, we measure gate voltage dependences. Figure 3A shows a color panel with voltage sweeps on gate 2. The main observation is the occurrence of two opposite types of behavior. First, we observe peaks in the density of states that change with energy when changing gate voltage (e.g., highlighted with dotted lines), these are the same resonances as shown in Fig. 2B and analyzed in (20). The second observation is that the ZBP from Fig. 2, which we take at 175 mT, remains stuck to zero bias while changing the gate voltage over a range of several volts. Clearly, our gates work since they change the Andreev bound states by ~ 0.2 meV per Volt on the gate. Panels (B) and (C) underscore this observation with voltage sweeps on a different gate, number 4. (B) shows that at zero magnetic field no ZBP is observed. At 200 mT the ZBP becomes again visible in (C). Comparing the effect of gates 2 and 4, we observe that neither moves the ZBP away from zero.

Initially, Majorana fermions were predicted in single-subband, one-dimensional wires (8, 9), but further work extended these predictions to multi-subband wires (27–30). In the nanowire section that is uncovered we can gate tune the number of occupied subbands from 0 to ~ 4 with subband separations of several meV. Gate tuning in the nanowire section

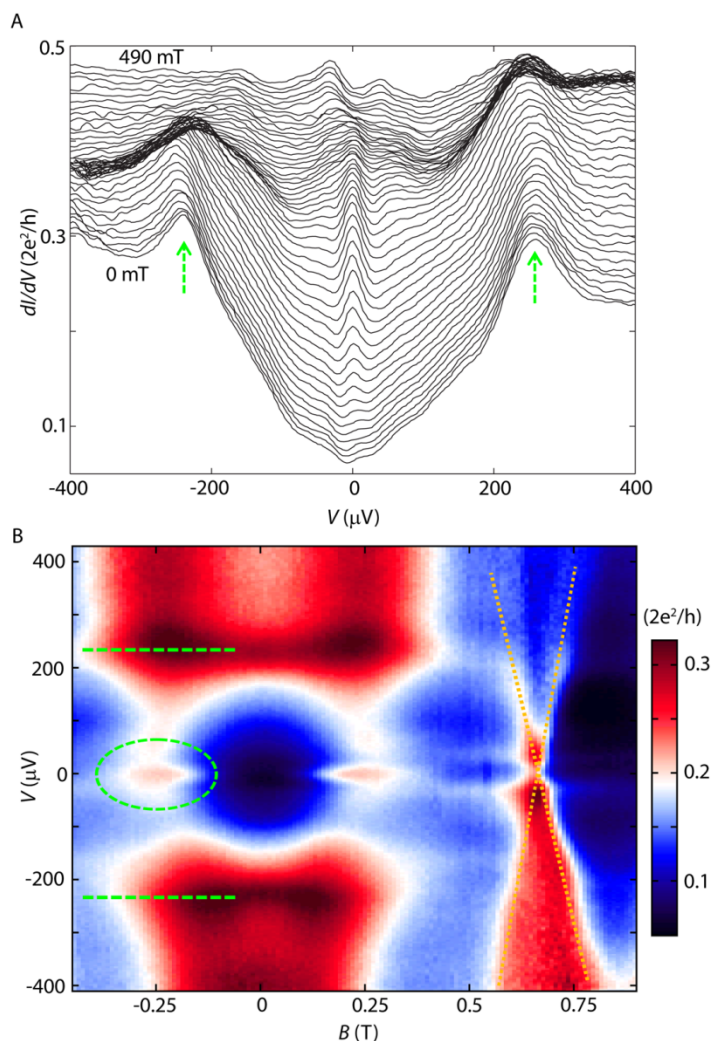


Fig. 2. Magnetic field dependent spectroscopy. (A) dI/dV versus V at 70 mK taken at different B -fields (from 0 to 490 mT in 10 mT steps; traces are offset for clarity, except for the lowest trace at $B = 0$). Data from device 1. (B) Color scale plot of dI/dV versus V and B . The zero-bias peak is highlighted by a dashed oval. Dashed lines indicate the gap edges. At ~ 0.6 T a non-Majorana state is crossing zero bias with a slope equal to ~ 3 meV/T (indicated by sloped dotted lines). Traces in (A) are extracted from (B).

covered with superconductor is much less effective due to efficient screening. The number of occupied subbands in this part is unknown, but it is most likely multi-subband. As shown in figs. S9 and S11 of (20) we do have to tune gate 1 and the tunnel barrier to the right regime in order to observe the ZBP.

We have measured in total several hundred panels sweeping various gates on different devices. Our main observations (20) are (i) ZBP exists over a substantial voltage range for every gate starting from the barrier gate until gate 4, (ii) we can occasionally split the ZBP in two peaks located symmetrically around zero, and (iii) we can never move the peak away from zero to finite bias. Data sets such as those in Figs. 2 and 3 demonstrate that the ZBP remains stuck to zero energy over considerable changes in B and gate voltage V_g .

Figure 3D shows the temperature dependence of the ZBP. We find

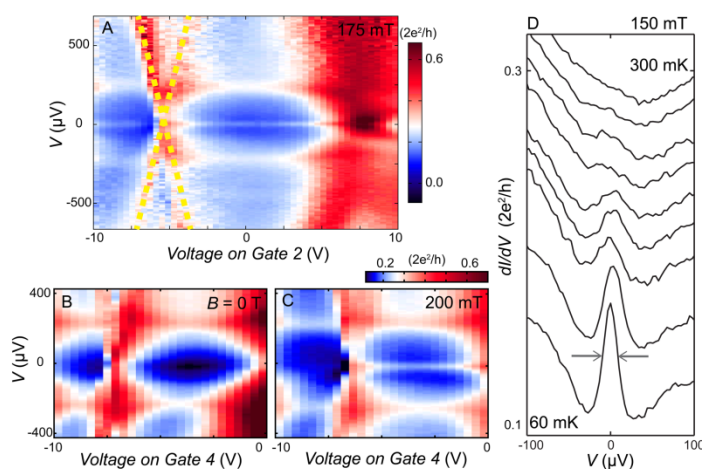


Fig. 3. Gate voltage dependence. (A) 2D color plot of dI/dV versus V and voltage on gate 2 at 175 mT and 60 mK. Andreev bound states cross through zero bias, for example near -5 V (dotted lines). The ZBP is visible from -10 to ~ 5 V (although in this color setting it is not equally visible everywhere). Split peaks are observed in the range of 7.5 to 10 V (20). In (B) and (C) we compare voltage sweeps on gate 4 for 0 and 200 mT with the zero bias peak absent and present, respectively. Temperature is 50 mK. [Note that in (C) the peak extends all the way to -10 V (19).] (D) Temperature dependence. dI/dV versus V at 150 mT. Traces have an offset for clarity (except for the lowest trace). Traces are taken at different temperatures (from bottom to top: 60, 100, 125, 150, 175, 200, 225, 250, and 300 mK). dI/dV outside ZBP at $V = 100$ μ eV is $0.12 \pm 0.01 \cdot 2e^2/h$ for all temperatures. A full-width at half-maximum of 20 μ eV is measured between arrows. All data in this figure are from device 1.

that the peak disappears at around ~ 300 mK, providing a thermal energy scale of $k_B T \sim 30$ μ eV. The full-width at half-maximum at the lowest temperature is ~ 20 μ eV, which we believe is a consequence of thermal broadening as $3.5 \cdot k_B T(60 \text{ mK}) = 18$ μ eV.

Next we verify explicitly that all the required ingredients in the theoretical Majorana proposals (Fig. 1A) are indeed essential for observing the ZBP. We have already verified that a nonzero B -field is needed. Now, we test if spin-orbit interaction is crucial for the absence or presence of the ZBP. Theory requires that the external B has a component perpendicular to B_{so} . We have measured a second device in a different setup containing a 3D vector magnet such that we can sweep the B field in arbitrary directions. In Fig. 4 we show dI/dV versus V while varying the angle for a constant field magnitude. In Fig. 4A the plane of rotation is approximately equal to the plane of the substrate. We clearly observe that the ZBP comes and goes with angle. The ZBP is completely absent around $\pi/2$, which thereby we deduce as the direction of B_{so} . In Fig. 4B the plane of rotation is perpendicular to B_{so} . Indeed we observe that the ZBP is now present for all angles, because B is now always perpendicular to B_{so} . These observations are in full agreement with expectations for the spin-orbit direction in our samples (17, 31). We have further verified that this angle dependence is not a result of the specific magnitude of B or a variation in g -factor (20).

As a last check we have fabricated and measured a device of identical design but with the superconductor replaced by a normal Au contact (i.e., a N-NW-N geometry). In this sample we have not found any signature of a peak that sticks to zero bias while changing both B and V_g (20).

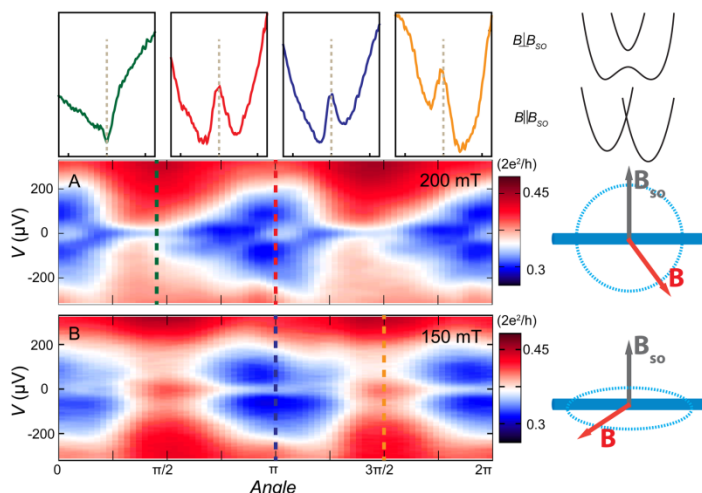


Fig. 4. Magnetic field orientation dependence. dI/dV versus V and varying the angle of B at fixed magnitude. Data from device 2 measured in a different setup at ~ 150 mK. Zero angle is along the nanowire for both panels. **(A)** Rotation of $|B| = 200$ mT in the plane of the substrate. The ZBP is maximum when B is parallel and absent when B is perpendicular to the wire. **(B)** Rotation of $|B| = 150$ mT in the plane perpendicular to B_{so} . The ZBP is now present for all angles. The panels on top show linecuts at angles with corresponding colors in (A) and (B). Panels on the right side illustrate from top to bottom: (1) For B perpendicular to B_{so} a gap opens lifting fermion doubling, as is required for Majoranas, (2) For B parallel to B_{so} the two spin bands from Fig. 1A shift vertically by $2E_z$. In this configuration a zero-energy Majorana is not expected, (3) panel of rotation of B for data in (A), (4) panel of rotation of B for data in (B).

This test experiment shows that superconductivity is indeed also an essential ingredient for our ZBP.

To summarize, we have reproduced in three different devices and in two different setups our observation of a rigid ZBP. Our general observations are: (i) a ZBP appears at finite B and sticks to zero bias over a range from 0.07 to 1 T, (ii) the ZBP remains at zero bias while changing the voltage on any of our gates over significant ranges, (iii) the ZBP comes and goes with the angle of the B field with respect to the wire axis, which is in agreement with the expected spin-orbit interaction, (iv) the rigid ZBP is absent when the superconductor is replaced by a normal conductor. Based on these observations we conclude that our spectroscopy experiment provides evidence for the existence of Majorana fermions.

Improving the electron mobility and optimizing the gate coupling will enable mapping out the phase diagram of the topological superconductor in the plane of E_z and μ (27–30). It will be interesting to control the subband occupation underneath the superconductor down to a single subband in order to make direct comparisons to theoretical models. Currently, we probe induced gaps and states from all occupied subbands, each with a different coupling to the tunnel barrier. The topological state in the topmost subband likely has the weakest coupling to the tunnel barrier. Single subband models (8, 9) predict that one should observe a closing of the topological gap, however, in multi-subband systems this gap closing may not be visible. The constant gap in Fig. 2 may come from lower subbands. The presence of multi-subbands together with our finite temperature may also be the reason that our ZBP is currently only

$\sim 5\%$ of the theoretical zero-temperature limit of $2e^2/h$ (12, 14).

Finally, we note that this work does not address the topological properties of Majorana fermions. The first step toward demonstrating topological protection would be the observation of conductance quantization (12, 32). Second, in a Josephson tunnel junction with phase difference ϕ and with a pair of Majorana's on either side, the current-phase relation becomes proportional to $\sin(\phi/2)$. The factor 2 is another distinct Majorana signature, which should be observable as an h/e flux periodicity in a SQUID measurement (8, 9). The last type of experiment involves the exchange of Majorana's around each other. Such braiding experiments can reveal their non-Abelian statistics, which is the ultimate proof of topologically protected Majorana fermions (33–35).

References and Notes

1. E. Majorana, A symmetric theory of electrons and positrons. *Soryushiron Kenkyu* (Engl. transl.) **63**, 149 (1981) [translation from *Teoria simmetrica dell'elettrone e del positrone. Nuovo Cimento* **14**, 171 (1937)].
2. F. Wilczek, Majorana returns. *Nat. Phys.* **5**, 614 (2009). doi:10.1038/nphys1380
3. M. Franz, Race for Majorana fermions. *Physics* **3**, 24 (2010). doi:10.1103/Physics.3.24
4. A. Yu. Kitaev, Unpaired Majorana fermions in quantum wires. *Phys. Usp.* **44**, 131 (2001). doi:10.1070/1063-7869/44/10S/S29
5. L. Fu, C. L. Kane, Superconducting proximity effect and majorana fermions at the surface of a topological insulator. *Phys. Rev. Lett.* **100**, 096407 (2008). doi:10.1103/PhysRevLett.100.096407 Medline
6. J. D. Sau, R. M. Lutchyn, S. Tewari, S. Das Sarma, Generic new platform for topological quantum computation using semiconductor heterostructures. *Phys. Rev. Lett.* **104**, 040502 (2010). doi:10.1103/PhysRevLett.104.040502 Medline
7. J. Alicea, Majorana fermions in a tunable semiconductor device. *Phys. Rev. B* **81**, 125318 (2010). doi:10.1103/PhysRevB.81.125318
8. R. M. Lutchyn, J. D. Sau, S. Das Sarma, Majorana fermions and a topological phase transition in semiconductor-superconductor heterostructures. *Phys. Rev. Lett.* **105**, 077001 (2010). doi:10.1103/PhysRevLett.105.077001 Medline
9. Y. Oreg, G. Refael, F. von Oppen, Helical liquids and Majorana bound states in quantum wires. *Phys. Rev. Lett.* **105**, 177002 (2010). doi:10.1103/PhysRevLett.105.177002 Medline
10. For a review see: C. W. J. Beenakker, Search for Majorana fermions in superconductors. <http://arxiv.org/abs/1112.1950> (2011).
11. For a review see: J. Alicea, New directions in pursuit of Majorana fermions in solid state systems. <http://arxiv.org/abs/1202.1293> (2012).
12. K. T. Law, P. A. Lee, T. K. Ng, Majorana fermion induced resonant Andreev reflection. *Phys. Rev. Lett.* **103**, 237001 (2009). doi:10.1103/PhysRevLett.103.237001 Medline
13. K. Flensberg, Tunneling characteristics of a chain of Majorana bound states. *Phys. Rev. B* **82**, 180516 (2010). doi:10.1103/PhysRevB.82.180516
14. J. D. Sau, S. Tewari, R. Lutchyn, T. Stanescu, S. Das Sarma, Non-Abelian quantum order in spin-orbit-coupled semiconductors: Search for topological Majorana particles in solid-state systems. *Phys. Rev. B* **82**, 214509 (2010). doi:10.1103/PhysRevB.82.214509
15. S. R. Plissard *et al.*, From InSb nanowires to nanocubes: Looking for the sweet spot. *Nano Lett.* (2012); <http://pubs.acs.org/doi/abs/10.1021/nl203846g>
16. H. A. Nilsson *et al.*, Giant, level-dependent g factors in InSb nanowire quantum dots. *Nano Lett.* **9**, 3151 (2009). doi:10.1021/nl901333a Medline
17. S. Nadj-Perge *et al.*, Spectroscopy of spin-orbit quantum bits in indium antimonide nanowires. <http://arxiv.org/abs/1201.3707> (2012).
18. P. W. Brouwer, M. Duckheim, A. Romito, F. von Oppen, Probability distribution of Majorana end-state energies in disordered wires. *Phys. Rev. Lett.* **107**, 196804 (2011). doi:10.1103/PhysRevLett.107.196804 Medline
19. J. D. Sau, S. Tewari, S. Das Sarma, Experimental and materials considerations for the topological superconducting state in electron- and hole-doped semiconductors: Searching for non-Abelian Majorana modes in 1D nanowires and 2D heterostructures. *Phys. Rev. B* **85**, 064512 (2012). doi:10.1103/PhysRevB.85.064512
20. See supplementary materials on Science Online.
21. J. D. Pillet *et al.*, Andreev bound states in supercurrent-carrying carbon nanotubes revealed. *Nat. Phys.* **6**, 965 (2010). doi:10.1038/nphys1811
22. T. Dirks *et al.*, Transport through Andreev bound states in a graphene

- quantum dot. *Nat. Phys.* **7**, 386 (2011). [doi:10.1038/nphys1911](https://doi.org/10.1038/nphys1911)
23. H. le Sueur, P. Joyez, H. Pothier, C. Urbina, D. Esteve, Phase controlled superconducting proximity effect probed by tunneling spectroscopy. *Phys. Rev. Lett.* **100**, 197002 (2008). [doi:10.1103/PhysRevLett.100.197002](https://doi.org/10.1103/PhysRevLett.100.197002) [Medline](#)
 24. S. Sasaki *et al.*, Kondo effect in an integer-spin quantum dot. *Nature* **405**, 764 (2000). [doi:10.1038/35015509](https://doi.org/10.1038/35015509) [Medline](#)
 25. M. Zareyan, W. Belzig, Yu. V. Nazarov, Superconducting proximity effect in clean ferromagnetic layers. *Phys. Rev. B* **65**, 184505 (2002). [doi:10.1103/PhysRevB.65.184505](https://doi.org/10.1103/PhysRevB.65.184505)
 26. B. J. van Wees, P. de Vries, P. Magnée, T. M. Klapwijk, Excess conductance of superconductor-semiconductor interfaces due to phase conjugation between electrons and holes. *Phys. Rev. Lett.* **69**, 510 (1992). [doi:10.1103/PhysRevLett.69.510](https://doi.org/10.1103/PhysRevLett.69.510) [Medline](#)
 27. M. Wimmer, A. R. Akhmerov, M. V. Medvedeva, J. Tworzydło, C. W. Beenakker, Majorana bound states without vortices in topological superconductors with electrostatic defects. *Phys. Rev. Lett.* **105**, 046803 (2010). [doi:10.1103/PhysRevLett.105.046803](https://doi.org/10.1103/PhysRevLett.105.046803) [Medline](#)
 28. A. C. Potter, P. A. Lee, Multichannel generalization of Kitaev's Majorana end states and a practical route to realize them in thin films. *Phys. Rev. Lett.* **105**, 227003 (2010). [doi:10.1103/PhysRevLett.105.227003](https://doi.org/10.1103/PhysRevLett.105.227003) [Medline](#)
 29. R. M. Lutchyn, T. D. Stanescu, S. Das Sarma, Search for Majorana fermions in multiband semiconducting nanowires. *Phys. Rev. Lett.* **106**, 127001 (2011). [doi:10.1103/PhysRevLett.106.127001](https://doi.org/10.1103/PhysRevLett.106.127001) [Medline](#)
 30. T. D. Stanescu, R. M. Lutchyn, S. Das Sarma, Majorana fermions in semiconductor nanowires. *Phys. Rev. B* **84**, 144522 (2011). [doi:10.1103/PhysRevB.84.144522](https://doi.org/10.1103/PhysRevB.84.144522)
 31. P. Štředa, P. Šeba, Antisymmetric spin filtering in one-dimensional electron systems with uniform spin-orbit coupling. *Phys. Rev. Lett.* **90**, 256601 (2003). [doi:10.1103/PhysRevLett.90.256601](https://doi.org/10.1103/PhysRevLett.90.256601) [Medline](#)
 32. M. Wimmer, A. R. Akhmerov, J. P. Dahlhaus, C. W. J. Beenakker, Quantum point contact as a probe of a topological superconductor. *New J. Phys.* **13**, 053016 (2011). [doi:10.1088/1367-2630/13/5/053016](https://doi.org/10.1088/1367-2630/13/5/053016)
 33. N. Read, D. Green, Paired states of fermions in two dimensions with breaking of parity and time-reversal symmetries and the fractional quantum Hall effect. *Phys. Rev. B* **61**, 10267 (2000). [doi:10.1103/PhysRevB.61.10267](https://doi.org/10.1103/PhysRevB.61.10267)
 34. D. A. Ivanov, Non-Abelian statistics of half-quantum vortices in p -wave superconductors. *Phys. Rev. Lett.* **86**, 268 (2001). [doi:10.1103/PhysRevLett.86.268](https://doi.org/10.1103/PhysRevLett.86.268) [Medline](#)
 35. C. Nayak, S. H. Simon, A. Stern, M. Freedman, S. Das Sarma, Non-Abelian anyons and topological quantum computation. *Rev. Mod. Phys.* **80**, 1083 (2008). [doi:10.1103/RevModPhys.80.1083](https://doi.org/10.1103/RevModPhys.80.1083)
 36. C. Bena, Metamorphosis and taxonomy of Andreev bound states. <http://arxiv.org/abs/1107.2228> (2011).
 37. H. A. Nilsson, P. Samuelsson, P. Caroff, H. Q. Xu, Supercurrent and multiple Andreev reflections in an InSb nanowire Josephson junction. *Nano Lett.* **12**, 228 (2012). [doi:10.1021/nl203380w](https://doi.org/10.1021/nl203380w) [Medline](#)

Acknowledgments: We thank D. Thoen and T. Klapwijk for sharing their NbTiN technology. For discussions and assistance we thank A. Akhmerov, J. Alicea, C. Beenakker, M. Freedman, F. Hassler, G. Immink, H. Keijzers, C. Marcus, S. Nadj-Perge, Y. Nazarov, I. van Weperen, M. Wimmer, D. van Woerkom. This work has been supported by ERC, NWO/FOM Netherlands Organization for Scientific Research and Microsoft Corporation Station Q.

Supplementary Materials

www.sciencemag.org/cgi/content/full/science.1222360/DC1

Supplementary Text

Figs. S1 to S14

References (36, 37)

Data Files

23 March 2012; accepted 5 April 2012

Published online 12 April 2012; 10.1126/science.1222360